MWP phase shifters integrated in PbS-SU8 waveguides

Javier Hervás,[1,*] Isaac Suárez,[2] Joaquín Pérez,[1] Pedro J. Rodríguez Cantó,[3] Rafael Abargues,[3] Juan P. Martínez-Pastor,[2] Salvador Sales,[1] and José Capmany[1]

[1]*iTEAM Research Institute, Optical Quantum and Communications Group, Universitat Politécnica de Valencia, 46022 Valencia, Spain*

[2]*UMDO, Instituto de Ciencia de los Materiales, Universitat de Valencia, 46071 Valencia, Spain*

[3]*Intenanomat S.L, C/ Catedrático José Beltrán 2, 46980 Paterna, Spain*

[*]*jaherpe2@teleco.upv.es*

Abstract: We present new kind of microwave phase shifters (MPS) based on dispersion of PbS colloidal quantum dots (QDs) in commercially available photoresist SU8 after a ligand exchange process. Ridge PbS-SU8 waveguides are implemented by integration of the nanocomposite in a silicon platform. When these waveguides are pumped at wavelengths below the band-gap of the PbS QDs, a phase shift in an optically conveyed (at 1550 nm) microwave signal is produced. The strong light confinement produced in the ridge waveguides allows an improvement of the phase shift as compared to the case of planar structures. Moreover, a novel ridge bilayer waveguide composed by a PbS-SU8 nanocomposite and a SU8 passive layer is proposed to decrease the propagation losses of the pump beam and in consequence to improve the microwave phase shift up to 36.5° at 25 GHz. Experimental results are reproduced by a theoretical model based on the slow light effect produced in a semiconductor waveguide due to the coherent population oscillations. The resulting device shows potential benefits respect to the current MPS technologies since it allows a fast tunability of the phase shift and a high level of integration due to its small size.

OCIS codes: (130.5460) Polymer waveguides; (160.4236) Nanomaterials; (230.5590) Quantum-well, -wire and -dot devices; (310.2785) Guided wave applications; (350.4010) Microwaves.

References and links

1. J. Capmany and D. Novak, "Microwave photonics combines two worlds," Nat. Photonics **1**(6), 319–330 (2007).
2. J. Yao, "Microwave photonics," J. Lightwave Technol. **27**(3), 314–335 (2009).
3. M. H. Song, C. M. Long, R. Wu, D. S. Seo, D. E. Leaird, and A. M. Weiner, "Reconfigurable and tunable flat-top microwave photonic filters utilizing optical frequency combs," IEEE Photon. Technol. Lett. **23**(21), 1618–1620 (2011).
4. J. Capmany, J. Mora, I. Gasulla, J. Sancho, J. Lloret, and S. Sales, "Microwave photonic signal processing," J. Lightwave Technol. **31**(4), 571–586 (2013).
5. D. Marpaung, C. Roeloffzen, R. Heideman, A. Leinse, S. Sales, and J. Capmany, "Integrated microwave photonics," Laser & Photon. Rev. **7**(4), 506–538 (2013).
6. R. J. Mailloux, *Phased Array Antenna Handbook*, (Artech House, 2005).
7. R. Minasian, "Photonic Signal Processing of Microwave Signals," IEEE Trans. Microw. Theory Tech. **54**(2), 832–846 (2006).
8. M. Pagani, D. Marpaung, and B. J. Eggleton, "Ultra-wideband microwave photonic phase shifter with configurable amplitude response," Opt. Lett. **39**(20), 5854–5857 (2014).
9. A. Loayssa and F. J. Lahoz, "Broad-band RF photonic phase shifter and single-sideband modulation," IEEE Photon. Technol. Lett. **18**(1), 208–210 (2006).
10. M. Pagani, D. Marpaung, and B. J. Eggleton, "Ultra-wideband microwave photonic phase shifter with configurable amplitude response," Opt. Lett. **39**(20), 5854–5857 (2014).

#235062 - $15.00 USD Received 24 Feb 2015; revised 1 Apr 2015; accepted 2 Apr 2015; published 22 May 2015

11. A. Meehan and M. Connelly, *"Slow light based microwave photonic phase shifter using coherent population oscillations in a bulk tensile-strained semiconductor optical amplifier,"* in Proc. of the 25th IET ISSC 2014/CIICT 2014 (IET, 2014), pp. 328–330.
12. W. Xue, S. Sales, J. Capmany, and J. Mørk, "Wideband 360 degrees microwave photonic phase shifter based on slow light in semiconductor optical amplifiers," Opt. Express **18**(6), 6156–6163 (2010).
13. M. Pu, L. Liu, W. Xue, Y. Ding, H. Ou, K. Yvind, and J. M. Hvam, "Widely tunable microwave phase shifter based on silicon-on-insulator dual-microring resonator," Opt. Express **18**(6), 6172–6182 (2010).
14. M. Burla, D. Marpaung, L. Zhuang, C. Roeloffzen, M. R. Khan, A. Leinse, M. Hoekman, and R. Heideman, "On-chip CMOS compatible reconfigurable optical delay line with separate carrier tuning for microwave photonic signal processing," Opt. Express **19**(22), 21475–21484 (2011).
15. H. Shahoei and J. Yao, "Tunable microwave photonic phase shifter based on slow and fast light effects in a tilted fiber Bragg grating," Opt. Express **20**(13), 14009–14014 (2012).
16. M. Pagani, D. Marpaung, D. Y. Choi, S. J. Madden, B. Luther-Davies, and B. J. Eggleton, "Tunable wideband microwave photonic phase shifter using on-chip stimulated Brillouin scattering," Opt. Express **22**(23), 28810–28818 (2014).
17. I. Suárez, H. Gordillo, R. Abargues, S. Albert, and J. Martínez-Pastor, "Photoluminescence waveguiding in CdSe and CdTe QDs-PMMA nanocomposite films," Nanotechnology **22**(43), 435202 (2011).
18. A. L. Ricchiuti, I. Suárez, D. Barrera, P. J. Rodríguez-Canto, C. R. Fernández-Pousa, R. Abargues, S. Sales, J. Martínez-Pastor, and J. Capmany, "Colloidal quantum dots-PMMA waveguides as integrable microwave photonic phase shifter," IEEE Photon. Technol. Lett. **26**(4), 402–404 (2014).
19. H. Gordillo, I. Suárez, R. Abargues, P. J. Rodríguez-Cantó, S. Albert, and J. P. Martínez-Pastor, "Polymer/QDs nanocomposites for waveguiding applications," J. Nanomater. **2012**, 960201 (2012).
20. H. Gordillo, I. Suárez, R. Abargues, P. J. Rodríguez-Cantó, and J. P. Martínez-Pastor, "Quantum-dot double layer polymer waveguides by evanescent light coupling," J. Lightwave Technol. **31**(15), 2515–2525 (2013).
21. W. W. Yu and X. Peng, "Formation of high-quality CdS and other II-VI semiconductor nanocrystals in noncoordinating solvents: Tunable reactivity of monomers," Angew. Chem. Int. Ed. Engl. **41**(13), 2368–2371 (2002).
22. B. De Geyter, Y. Justo, I. Moreels, K. Lambert, P. F. Smet, D. Van Thourhout, A. J. Houtepen, D. Grodzinska, C. de Mello Donega, A. Meijerink, D. Vanmaekelbergh, and Z. Hens, "The different nature of band edge absorption and emission in colloidal PbSe/CdSe core/shell quantum dots," ACS Nano **5**(1), 58–66 (2011).
23. MicroChem Corp, http://www.microchem.com/Prod-SU-8_KMPR.htm
24. L. Arques, A. Carrascosa, V. Zamora, A. Díez, J. L. Cruz, and M. V. Andrés, "Excitation and interrogation of whispering-gallery modes in optical microresonators using a single fused-tapered fiber tip," Opt. Lett. **36**(17), 3452–3454 (2011).
25. H. Gordillo, I. Suárez, R. Abargues, P. J. Rodríguez-Cantó, and J. P. Martínez-Pastor, "Color tuning and white light by dispersing CdSe, CdTe, and CdS in PMMA nanocomposite waveguides," IEEE Photon. J. **5**(2), 2201412 (2013).
26. I. Suárez, A. Larrue, P. J. Rodríguez-Cantó, G. Almuneau, R. Abargues, V. S. Chirvony, and J. P. Martínez-Pastor, "Efficient excitation of photoluminescence in a two-dimensional waveguide consisting of a quantum dot-polymer sandwich-type structure," Opt. Lett. **39**(16), 4962–4965 (2014).
27. J. Mørk, R. Kjær, M. van der Poel, and K. Yvind, "Slow light in a semiconductor waveguide at gigahertz frequencies," Opt. Express **13**(20), 8136–8145 (2005).
28. G. Lifante, *Integrated Photonics Fundamentals* (John Wiley and Sons, 2003).

1. Introduction

Microwave photonics (MWP) [1] enables the broadband, interference-immune and low loss transport and processing of radiofrequency and millimeter-wave signals conveyed by optical carriers opening the possibility of multiple functionalities which are key in a considerable number of application fields such as fiber-wireless communication and 5G networks, radar, signal filtering, sensing or instrumentation [2]. Moreover, an additional advantage of MWP systems is that they enable to perform RF functionalities, such as fast tunability or reconfigurability, that are either complex or not even possible to achieve with conventional RF architectures [3]. These potential practical functionalities include as well arbitrary waveform generation, tunable and reconfigurable filtering, optoelectronic oscillators, analog to digital conversion or beam steering, among others. These complex operations are based on basic functions, such as tunable true-time delay (TTD), splitting/combining and phase shifting (PS) [4,5] and MWP solutions provide broadband performance and enhanced tunability on TTD and PSs. Moreover, the processing of microwave signals using photonic integrated circuits (PICs) known as integrated microwave photonics (IMWP) is bringing additional

#235062 - $15.00 USD Received 24 Feb 2015; revised 1 Apr 2015; accepted 2 Apr 2015; published 22 May 2015

advantages such as compactness, reproducibility and reduced costs of the CMOS foundry processes in order to provide a real flexibility to microwave photonic signal processors [5].

One fundamental building block of practical MWP functionalities, e.g., beam forming, filtering, signal generation, is the microwave phase shifter (MPS) [6]. Despite of the different architectures presented in the literature, the use of photonics for processing microwave signals may overcome the limitations of electronic PSs, namely frequency-dependent loss and dispersion, to enable ultra wideband operation [7,8]. Examples of photonic MPS architectures or technologies are the use of stimulated Brillouin scattering (SBS) [9,10] or the SOA based implementation [11], whose working principle is based on the slow and fast light phenomenon due to coherent population oscillation (CPO) [12]. Besides, silicon on insulator (SOI) ring resonators have been used to perform the same functionality in narrowband systems [13,14], and fiber Bragg gratings have also been proposed to accurately tune the phase-shift (FBGs) [15]. However, although these technologies allow an efficient control of the microwave phase shift they also present some drawbacks that may limit their practical applications. For instance, SBS based phase shifters require both long fiber sections or high pump powers [16], SOA based architectures have distortion and RIN noise limitations while the SOI ring and FBG approximations feature a narrowband behavior.

To overcome those constraints here we proposed a novel technology approach that is able to integrate photonic MPS with organic waveguides implemented in silicon platforms. This new technology consists of nanocomposites made by the dispersion of colloidal quantum dots (QD) in polymers [17]. Such a multicomponent material is emerging as a very suitable candidate to develop novel functionalities in photonic devices. The reason comes from the fact that nanocomposites combine the singular optical properties of the QDs (room temperature emission and band-gap tunability) with the technological feasibilities of polymers, i.e. deposition on films by different coating methods, patterning by UV or e-beam lithography, among others. Indeed, we have already demonstrated that planar waveguides, as depicted in Fig. 1(a), fabricated by the dispersion of PbS QDs in polymethylmethacrylate (PMMA) can induce a phase shift over microwave signals carried at 1550 nm when the structure is pumped at 980 nm, where the QDs show significant absorption [18]. Nevertheless, integrated photonic technology on general and integrated microwave photonics in particular requires not only planar structures, but also lateral light confinement structures to improve the light-matter interaction in order to design more complex devices and functionalities. Among the different patterning techniques, UV photolithography is the most appropriate to fabricate 2D waveguides when widths are ranged between 1 and 20 μm. For these purposes the epoxy-based negative photoresist SU8 is the most used for 2D waveguiding applications because it shows a high refractive index (~1.5) together with low propagation losses in the 600-1600 nm range [19]. However, SU8 shows poor chemical compatibility with as-synthesized oleate capped QDs because SU8 is typically formulated with γ-butyrolactone or cyclopentanone, where oleate-capped QDs are not soluble.

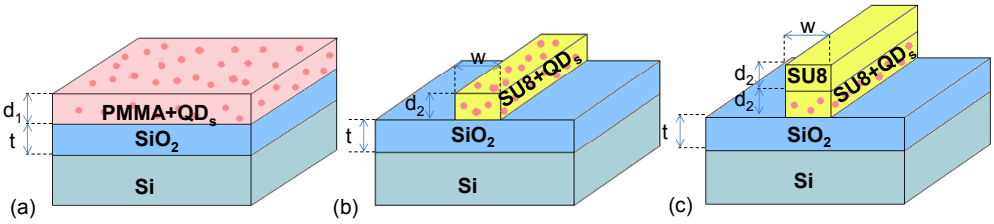

Fig. 1. Schematic view of the waveguides studied: a) PMMA based waveguide, b) SU8 monolayer waveguide and c) SU8 bilayer waveguide.

In this way, we here propose an appropriate ligand exchange procedure to modify the QD surface and make them soluble in SU8 solvents [19]. By means of the ligand exchange approach, bidimensional QD-SU8 waveguides were successfully fabricated and used as a

#235062 - $15.00 USD Received 24 Feb 2015; revised 1 Apr 2015; accepted 2 Apr 2015; published 22 May 2015

novel MPS, as shown in Fig. 1(b). These structures improve the results obtained with QD-PMMA waveguides published in [18] under the same pumping conditions due to a better confinement of the light thanks to the proposed QD-SU8 monolayer waveguide structure. Moreover, we have already demonstrated that propagation of light along the waveguides is improved depositing passive claddings on the top of the nanocomposite [18,20]. Thus, a novel bidimensional waveguide consisting of a bilayer structure composed by a QD-SU8 layer and a SU8 cladding layer is also proposed, as shown in Fig. 1(c), to decrease the losses of the light and hence to improve the microwave phase shift up to 40°. In addition, the proposed structure adds a new flexibility level, as is the waveguide width, to face different on chip requirements. Moreover a refractive index model of the PbS-SU8 nanocomposite is implemented, where main results are explained by considering the absorption saturation produced in the QDs and developing a model able to fit accurately the experimental data.

2. Waveguide structure and fabrication

The nanocomposites used in this work are based on the dispersion of PbS QDs in PMMA and SU8 matrices. Nanocrystals were synthetized following the method previously reported by Yu and Peng [21]. The QD diameter was about 4.5 nm [22], which corresponds to an exciton absorption peak close to 1550 nm -see inset of Fig. 2- and hence providing efficient absorption at this wavelength [18]. Then, the different QD-polymer nanocomposites structures were fabricated on a SiO_2/Si substrate (2 μm of SiO_2) in order to provide a high refractive index contrast in the active material (around 2% respect the SiO_2). The filling factor (*ff*) of nanocrystals into the polymer was formulated to be around 10^{-3} to obtain a good compromise between QD excitation and light absorption [17]. The first structure depicted in Fig. 1(a) consisted in a planar waveguide composed by a d_1 = 3 μm thick PbS-PMMA film. This nanocomposite was formulated by dissolving the PbS QDs and PMMA in toluene. Afterwards, the planar waveguide was fabricated by spin-coating the PbS-PMMA solution on the substrate and post baking the sample at 80 °C and 150 °C for two minutes each [17].

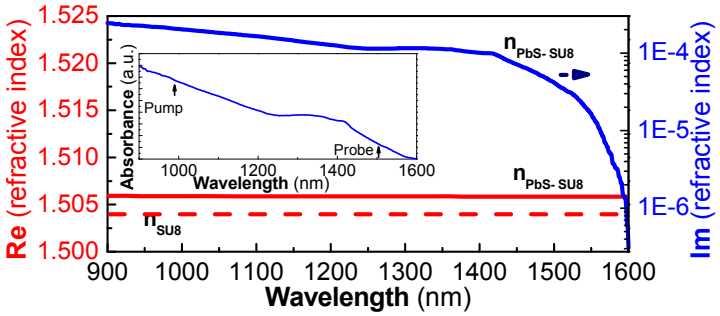

Fig. 2. Real (red solid line) and imaginary (blue solid line) parts of the PbS-SU8 (ff = 0.01) refractive index and real (red dashed line) part of the SU8 refractive index. The inset shows the absorption spectra of the PbS-SU8 QDs at pump (980 nm) and probe (1550 nm) wavelengths.

In the second design shown in Fig. 1(b), active straight ridge waveguides were implemented by dispersing the PbS QDs in SU8. For this purpose, it was necessary to perform a surface modification of the QDs to make them soluble and to allow a good dispersion of the nanocrystals in γ-butyrolactone [19]. Then, straight ridge waveguides were fabricated upon UV exposure following the standard procedure explained in [23]. A d_1 = 2.5 μm PbS-SU8 film was firstly spin-coated on the nanocomposite and baked in two steps at 65 °C and 95 °C for two minutes each, respectively. This film was later exposed to the UV radiation for three seconds in a MJB4 Suss-Mikrotec mask aligner using a mask consisted in consecutive sets of w = 4, 6, 8, 10 and 20 μm wide lines with a 50 and 100 μm separation between lines and sets respectively. After illumination, the samples were post-baked at 65 and

#235062 - $15.00 USD Received 24 Feb 2015; revised 1 Apr 2015; accepted 2 Apr 2015; published 22 May 2015

95 °C for two minutes each, and finally they were developed for one minute. It is interesting to remark that the resist lithographic performance was not disturbed by the presence of the nanocrystals.

The last sample, shown in Fig. 1(c), is proposed to decrease the light losses travelling through the structure and consists in a ridge bilayer waveguide composed by a PbS-SU8 nanocomposite and a SU8 passive cladding layer. In these conditions, the light can propagate through the cladding without limitation of the QDs absorption and in consequence the signal-to-noise-ratio (SNR) is improved. A similar structure was firstly proposed in planar waveguides in [20], but here it is the first time where it is performed in patterned structure. The fabrication procedure followed the process used to implement QD-SU8 ridge waveguides, but the initial steps consisted in two spin coatings, first the PbS-SU8 nanocomposite and then the SU8. The thickness of both films were $d_1 = d_2 = 2$ μm. Finally, waveguides with a thickness $d_1 + d_2 = 4$ μm were well defined when the process was over.

Figure 2 plots the real (left axis) and imaginary part (right axis) of the PbS-SU8 composite refractive index calculated with the method explained in [17]. The real part is close to that of the SU8 (red dashed line) and the imaginary part follows the absorption curve of the PbS (see inset in the figure), which it is around ~10^{-5} at 1550 nm and increases for shorter wavelengths up to ~$2 \cdot 10^{-4}$ at 980 nm.

3. Experimental set-up and principle of operation

The setup used to perform the measurements is shown in Fig. 3. Initially, a 1550 nm continuous-wave (CW) laser is electro-optically modulated with a microwave tone (10 MHz - 25 GHz) generated by a vector network analyzer (VNA), part of a light component analyzer (LCA). Then, the generated optical double-side band signal at the optical LCA module is mixed together with a 980 nm CW pump laser, from a tunable laser source, at a wavelength division multiplexer (WDM). At the output of the WDM the two mixed beams are injected into the waveguide (WG) with the aid of a tapered fiber [24]. At the output edge of the WG sample, light is collected with another lensed fiber and pumped into the WDM in order to separate the optical beams and photodetect the modulated 1550 nm signal under interest. Also the 980 nm is measured only for control issues. Afterwards, the amplitude and phase of the detected electrical signal are captured by the electrical LCA module or VNA, where the scattering parameter S_{21} which relates the detected and generated MW signals is calculated.

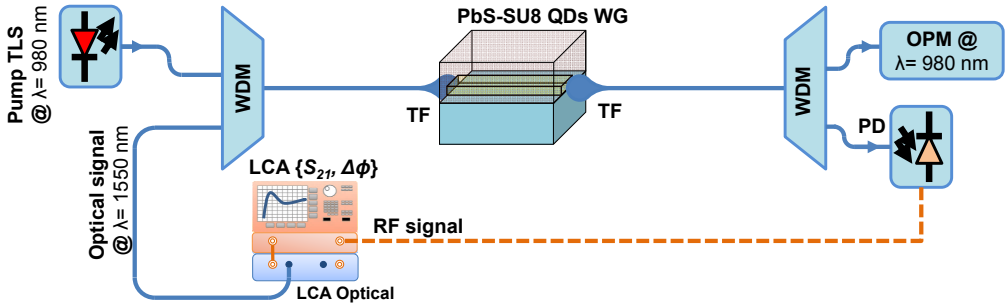

Fig. 3. Measurement laboratory setup. OPM: optical power meter, RF: radiofrequency, TLS: tunable laser source, PD: photodetector, TF: Tapered Fiber tip, WG: waveguide, LCA: light component analyzer.

The working principle of the phase-shifter is based on the saturable absorption of the QDs when they are pumped below their band-gap, where the nanocrystals show strong absorption, as shown in inset of Fig. 2. Therefore, when the light at 980 nm excites the QDs it is expected to affect the group index of the signal travelling at 1550 nm, producing a phase change (Δφ) in the microwave signal that can be expressed as:

#235062 - $15.00 USD Received 24 Feb 2015; revised 1 Apr 2015; accepted 2 Apr 2015; published 22 May 2015

$$\Delta\varphi = \Delta kL = \frac{\Omega}{c}\Delta n_g L, \tag{1}$$

being k the wave vector of the signal, L the length of the waveguide, Ω the angular frequency, c the speed of light and Δn_g the group refractive index variation.

4. Experimental characterization of the PbS-SU8 QDs waveguides

Samples with the structure shown in Figs. 1(a)-1(c) where tested as MPS by characterizing the microwave signal with the set-up explained in the last section. In order to make a comparison between the different structures, the pump and signal powers inside the waveguide were fixed to 3.64 and 1.6 mW respectively.

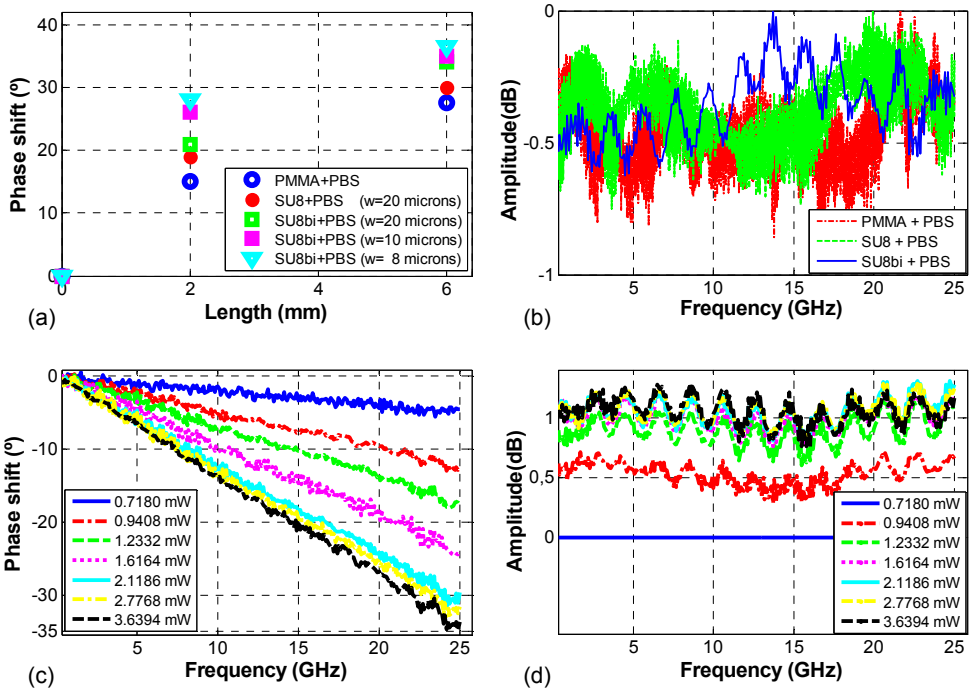

Fig. 4. a) Phase shifting at 25 GHz suffered by the MW signal for different waveguides with different widths and lengths and b) normalized RF amplitude response as a function of the microwave frequency for different waveguides structures with length 6 mm when they are pumped by the 980 nm laser under the highest output power. c) Phase shifting as a function of the microwave frequency and d) amplitude responses as a function of the microwave frequency in the 20 μm wide 6 mm long SU8 bilayer waveguide by pumping with the 980 nm laser for different coupled powers to the input edge of the structure normalized to the smallest pump power trace.

Figure 4(a) shows the phase shift recorded at the output edge of the different sample structures at 25 GHz for waveguide lengths of 2 and 6 mm. In all the measured cases, the phase shift increases with the waveguide length, but the curve deviates from the linear behavior predicted by Eq. (1) because of the attenuation of the pump beam along the structures, which prevents a uniform excitation of the nanocrystals [17]. The phase shift measured with the planar PbS-PMMA waveguide (blue symbols) is clearly improved by the ridge PbS-SU8 structure reaching 30 ° at the waveguide length of 6 mm. This is due to the fact that the ridge waveguides allow a better confinement of the light that leads to a power density increase and with it a higher light absorption by the nanocrystals.

#235062 - $15.00 USD Received 24 Feb 2015; revised 1 Apr 2015; accepted 2 Apr 2015; published 22 May 2015

However, this proposed waveguide suffers from high attenuation due to the absorption of the QDs, and the SNR results very weak for long waveguides. Nevertheless, the light attenuation is significantly reduced inducing an improvement in the SNR, as can be seen in Fig. 4(b), when a passive layer is deposited onto the active material [20]. Considering coupling losses of 10 dB, the total optical power losses estimated between the input and the end edge of the QD-SU8 bilayer waveguide were around 21 and 34 dB for the widest/smallest and the thinnest/longest waveguide respectively. However, the PMMA based waveguide structure losses are estimated around 33-44 dB (2 dB lower for the SU8 monolayer waveguides) because light can travel through the cladding, in the SU8 bilayer case, without absorption losses. In this way the proposed SU8 bilayer waveguides produced the better results. Green empty square, pink square and bright blue triangle symbols of Fig. 4(a) plot the phase shifts obtained with this waveguide structure for waveguide widths of 20, 10 and 8 μm respectively. The narrower the width, the higher the phase shifting due to the better confinement of the light, reaching a value of 36.5 ° for the thinner waveguide. Once the behavior of the phase shifter waveguide is established, its magnitude can be easily tuned by means of the pump power and the microwave frequency regarding a broadband operation. Figure 4(c) plots the phase shifting as a function of the microwave frequency in a 20 μm wide and 6 mm long SU8 bilayer waveguide for different pump powers. In this case, the phase shift increases with the microwave frequency according to Eq. (1) and also for growing pump powers, reaching saturation above 2 mW due to the saturation of the PbS QD absorption. Additionally, could be observed in Fig. 4(d) that the ripples in the amplitude response for different pump powers are lower than 0.5 dB. Moreover, there is a clear improvement of the RF amplitude signal for higher pump powers, proving that QDs are being saturated by the pump rather than the signal. The constant slope of phase shift at Fig. 4(c) implies a constant time delay in relation to those microwave frequencies. Therefore, the application of this phase shifter as true-time delay (TTD) device is straightforward from the proposed implementation principles and it would be considered for further investigation.

In this case, the phase shifting value obtained could be improved modifying the characterization set-up to obtain an enhanced confinement of the light and a higher excitation of the QDs on the PbS-SU8 material. In this case different strategies are being considered for further investigation. First, a dual light pumping from both sides of the waveguide sample could be interesting in order to improve light confinement and nanostructure excitation, but considering that a major concentration of QDs established a trade-off on the phase shifting [17]. Furthermore, it is possible to pump the nanostructures from the surface of the waveguide in order to provide a uniform excitation along the complete length of the structure [17,25]. This strategy imposes a higher complexity of the experimental set-up in the case of the dual light pumping, and requirements of high power lasers in the case of the surface pumping, because the excitation area is very large under these pumping conditions and hence the pump power density very low and usually insufficient to pump properly the nanocrystals. A second strategy could consist of improving the design of the sample in order to provide a major concentration of QDs together with low propagation losses. In this regard, we have recently demonstrated [26] a new two-dimensional waveguide consisting of a quantum dot-polymer sandwich-type structure. This structure is able to propagate the pump beam along PMMA claddings and to improve the efficiency of excitation about 100-fold compared with a similar one formed by dispersing homogeneously the QDs in the polymer. However, the application of this design with SU8 claddings is not straightforward and the appropriate technology to deposit the PbS QDs packed layer between the SU8 claddings together with keeping the lithographic properties is under investigation. Ultimately, these strategies that collect new experimental techniques and novel technological structure will allow an enhancement in excitation of QDs in a confined structure, and therefore translate into a significant phase shifting improvement.

#235062 - $15.00 USD Received 24 Feb 2015; revised 1 Apr 2015; accepted 2 Apr 2015; published 22 May 2015

5. Refractive index model for the PBs-SU8 QDs

The refractive index change can be explained with the slow light effect due to coherent population oscillations that takes places in a semiconductor when it is pumped by a strong field [27]. This effect produces a variation in the group velocity of the probe beam given by:

$$\Delta n_g = \frac{1}{2} c \tau_s \Gamma g_0 \frac{\left(\frac{\eta \cdot P}{P_{sat}}\right)}{\left(1+\frac{\eta \cdot P}{P_{sat}}\right)^3}, \tag{2}$$

where P is the carrier power, P_{sat} the carrier saturation power, τ_s the carrier lifetime, Γ the confinement factor of the mode, η the coupling efficiency and g_0 the modal gain without saturation related to the gain (g) of the waveguide by:

$$g = \frac{\Gamma g_0}{\left(1+\frac{P}{P_{sat}}\right)}. \tag{3}$$

In these conditions the light of the carrier beam follows the propagation equation:

$$\frac{dP}{dz} = \left(g - \alpha\right) \cdot P, \tag{4}$$

where α represents the losses at 1550 nm. Finally, the parameter g_0 is proportional to the pump power (P_p) [20] that also follows the propagation equation:

$$\frac{dP_P}{dz} = -\alpha_P \cdot P_P. \tag{5}$$

Thus, the change of the refractive index in the waveguide can be simulated solving together the Eqs. (2)-(5). The confinement factor (Γ) and the absorption losses (α and α_P) in the waveguide are estimated by analyzing the modes supported by the structure, which are calculated through the effective index method in the complex plane [28].

The former parameters are obtained from the imaginary part of the effective refractive index of the modes ($4 \cdot \pi \cdot \mathrm{Im}(N_{eff})/\lambda$). The later parameter is calculated integrating the mode overlap in the active region respect the entire mode area. In this way the algorithm found solutions of modes not only confined in the active, but also in the cladding layers. By considering a ff = 0.1% at λ = 980 nm, losses are found to be around 13 cm^{-1}. At λ = 1550 nm losses are reduced to 0.8 cm^{-1} because this wavelength is longer than that corresponding to the PbS quantum dot effective band-gap and the fundamental mode shows a confinement in the active region of around 65%.

#235062 - $15.00 USD Received 24 Feb 2015; revised 1 Apr 2015; accepted 2 Apr 2015; published 22 May 2015

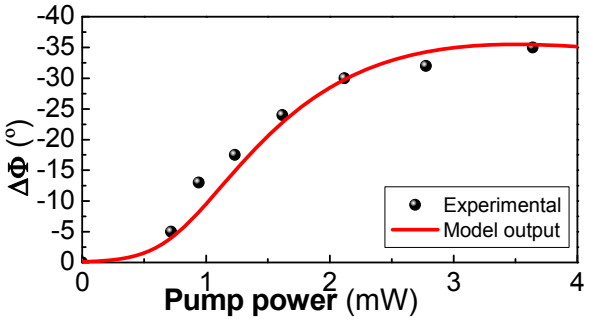

Fig. 5. Phase shift as a function of the pump power. Symbols correspond to experimental values and the red continuous line to the model output data.

Symbols of Fig. 5 show the experimental phase shifts as a function of the pump power fitted by the output data of the above described model (red line). Clearly, the model may reproduce nicely the experimental results. The parameters used were $g_0 = 0.022 \cdot P_P$, $\tau_s = 3.1$ ps, $\Gamma = 0.65$, $\alpha_p = 25$ cm^{-1}, $P_{sat} = 100$ mW and $\alpha_s = 6$ cm^{-1}. Higher losses considered in the fitting are attributed to the scattering of light in the polymer [19,25].

6. Conclusions

In this work a novel approach to implement a MPS based on a PbS-SU8 nanocomposite is reported, which is used to fabricate waveguides integrated into silicon platforms. For this purpose it was necessary to perform the appropriate ligand exchange to disperse the QDs homogeneously in the SU8 matrix. When PbS QDs are pumped below their absorption band-gap they are able to modify the group refractive index of an optical carrier at 1550 nm, producing in consequence a shift in the phase of the microwave signal. Moreover, lithographic properties of SU8 enable to define ridge patterns necessary to improve the confinement and the integration level. These PbS-SU8 waveguides exhibits a clear improvement of the phase shifting as compared to the value obtained for planar structures. Furthermore, a novel bilayer ridge structure consisting of a bottom PbS-SU8 nanocomposite and a top SU8 passive cladding is proposed to alleviate the pumping losses of the waveguide and in consequence to improve the phase shift up to 36.5 ° under current proposal. Nevertheless, we are currently working in other strategies to reach higher shifts. A first approach would be to increment the pump conditions to achieve a higher excitation of the QDs, and a second one to develop a novel technology able to deposit a PbS compact layer between two SU8 claddings. Then, we expect that such a novel structure together with the enhancement of the excitation conditions would improve the phase shifting in future investigations. Finally, to explain the experimental results a theoretical model able to reproduce the experimental data is proposed. The potential advantages of the proposed structures rely on a high level of integration and a continuous and fast tunability with the pump power and microwave frequency together under broadband operation.

Acknowledgments

The authors would like to thank Prof. Antonio Díez (Semiconductor and Fiber Optics group from the University of Valencia) for the fabrication of the tapered fiber tip. This work was supported in part by the Spanish MCINN through the projects TEC2011-29120-C05-05 and TEC2011-29120-C05-01, the financial support given by the Research Excellency Award Program GVA PROMETEO 2013/012, the EU-NAVOLCHI (project 288869) and the SEQMUST project under R+D+i joint resources and appreciation programme from the VLC/CAMPUS International Campus of Excellence supported by the Spanish MECD. J. Hervás work is supported by the MECD FPU scholarship (FPU13/04675) and J. Perez's work is supported by Spanish MINECO Juan de la Cierva Fellowship JCI-2012-14805.

#235062 - $15.00 USD Received 24 Feb 2015; revised 1 Apr 2015; accepted 2 Apr 2015; published 22 May 2015